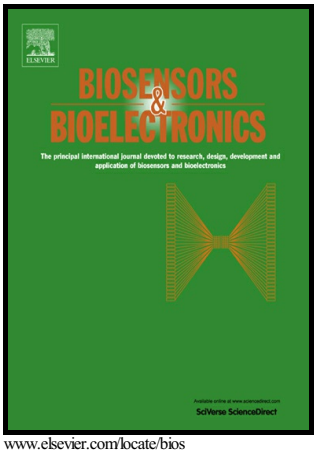

www.elsevier.com/locate/bios

Universal ratiometric electrochemical biosensing platform based on mesoporous platinum nanocomposite and nicking endonuclease assisted DNA walking strategy

Qinli Pu, Junlong Li, Juhui Qiu, Xuanhua Yang, Yi Li, Dan Yin, Xinyuan Zhang, Yiyi Tao, Shangchun Sheng, Guoming Xie

PII: S0956-5663(17)30232-4
DOI: http://dx.doi.org/10.1016/j.bios.2017.03.062
Reference: BIOS9650

To appear in: *Biosensors and Bioelectronic*

Received date: 18 November 2016
Revised date: 19 March 2017
Accepted date: 30 March 2017

Cite this article as: Qinli Pu, Junlong Li, Juhui Qiu, Xuanhua Yang, Yi Li, Dar Yin, Xinyuan Zhang, Yiyi Tao, Shangchun Sheng and Guoming Xie, Universa ratiometric electrochemical biosensing platform based on mesoporous platinur nanocomposite and nicking endonuclease assisted DNA walking strategy *Biosensors and Bioelectronic,* http://dx.doi.org/10.1016/j.bios.2017.03.062

Universal ratiometric electrochemical biosensing platform based on mesoporous platinum nanocomposite and nicking endonuclease assisted DNA walking strategy

Qinli Pu[a], Junlong Li[a], Juhui Qiu[b], Xuanhua Yang[c], Yi Li[a], Dan Yin[a], Xinyuan Zhang[a], Yiyi Tao[a], Shangchun Sheng[d], Guoming Xie[a*]

[a]Key Laboratory of Laboratory Medical Diagnostics of Education, Department of Laboratory Medicine, Chongqing Medical University, Chongqing 400016, P. R. China.

[b]State Key Laboratory of Membrane Biology, Tsinghua-Peking Center for Life Sciences, School of Life Sciences, Tsinghua University, Beijing 100084, P.R.China.

[c]Department of Gastrointestinal Surgery, Second Clinical Medical Institution of North Sichuan Medical College. Nanchong Central Hospital, Nanchong, Sichuan 637000,P.R. China.

[d]The No.2 Peoples' Hospital of Yibin, Sichuan, 644000, P.R. China.

guomingxie@cqmu.edu.cn

xiegm059@foxmail.com

[*]**Correspondence author:** Guoming Xie, Key Laboratory of Laboratory Medical Diagnostics of Education, Ministry of Education, Department of Laboratory Medicine, Chongqing Medical University, No. 1 Yi Xue Yuan Road, Chongqing 400016, PR China. Tel.: +86 23 68485240; Fax.: +86 23 68485240

Abstract

The occurrence and development of many complex diseases are associated with various molecules, whose contents are rarely in the early stage of the disease. Thus a universal platform for the ultrasensitive detection of multilevel biomarkers should be developed. In this study, we introduced an electrochemical biosensing system based on nicking endonuclease (Nt.BbvCI) assisted DNA walking strategy. We successfully constructed a universal signal-off-on ratiometric electrochemical biosensor for various biomolecules, including small molecules, nucleic acids, and proteins, by progressively optimizing the schematics (schemes 1, 2, and 3). The MB-hairpin probes (MB-HPs) acted as a signal-off probe, and nanocomposites (MPNs@DOX@DNA2) acted as a conventional signal-on probe (scheme 3). With the aid of the MPNs@DOX@DNA2 and Nt.BbvCI assisted DNA walking mechanism, the designed ratiometric electrochemical biosensor showed a high sensitivity and broad detection range. In addition, the proposed method can be utilized to detect diverse targets quantitatively by changing the sequence of aptamers under optimum experimental conditions. Furthermore, it has been widely proved to realize well-accepted signal response in identifying complex samples, thereby resulting in an wide prospect for bioanalysis and clinical diagnosis.

Keywords: Ratiometric electrochemical biosensor; Mesoporous platinum; Nicking endonuclease; DNA walking strategy.

1. Introduction

The early-stage diagnosis and treatment of various diseases largely rely on many low-abundance biomarkers in body fluids (Sawyers 2008), including small molecules at the metabolic level (Carta et al., 2015; Petersen and Verkhratsky 2016), proteins at the functional level (Dadrich et al., 2016; Loh et al., 2015; Shibuya 2013), and DNAs at the genetic level (Dopico et al., 2015; Pletscher-Frankild et al., 2015). Many biomolecular detection platforms, including enzyme-linked immunosorbent assay (ELISA) for detecting protein and small molecules (Berg et al., 2015; Toh et al., 2015), polymerase chain reaction (PCR) for nucleic acids (Banerjee et al., 2015; Innis et al., 2012), have been developed to determine individual types of molecular targets. Although these platforms are well suited for the selective detection of single-level biomarkers, they usually need costly apparatus, complicated pretreatment procedure, and trained personnel. Most importantly, they exhibit a limited detection ability at other molecular levels. Currently available single biomarkers cannot usually predict and evaluat the occurrence and prognosis of diseases accurately. Advances in genomics, proteomics, and metabolomics has been shown that complex diseases such as cancer are characteristics of multiple complex molecular events in disease

development and prognosis (Das et al., 2015; Kelley et al., 2014; Onda et al., 2016; Sreekumar et al., 2013; Tsai et al., 2013). Thus, a rapid, inexpensive, durable, ultrasensitive, and easy-operation platform should be developed to detect multiple-level biomarkers, which would facilitate the development of early diagnosis and precision medicine (Zheng et al., 2012).

In recent years, numerous universal platforms have been reported (Chen et al., 2015a; Li et al., 2015a; Lin et al., 2016; Linardy et al., 2016; Wu et al., 2016; Zhu et al., 2016). For example, Shuo Shi and colleagues (Zhu et al., 2016) developed a universal fluorescent aptasensor based on the recognition-induced conformational alteration of aptamer and a DNA-AgNC fluorescence light-up system, this system is fast and specific in detecting different biomolecules. However, AgNCs synthesis using DNA sequence as a template shows poor stability and reproducibility. Moreover, this proposed method also lacks a signal amplification system, hence its none-effectiveness for analysis of multiple low-abundance biomolecules. Chunhai Fan and coworkers (Lin et al., 2016) also developed a universal electrochemical sensor on DNA-nanostructure based programmable engineering of the biomolecular recognition interface. Although the tetrahedral DNA nanostructure (TDN)-based biosensing platform can selectively determine various types of molecules, a stable TDN is difficult to self-assemble. Therefore, the reproducibility

of the biosensor is largely dependent on TDNs. The poor sensitivity of the detection system also cannot meet the requirement of early-stage diagnosis for many complex diseases (Liu et al., 2014).

Currently, enzyme-assisted DNA walking machines have attracted considerable attention. To enable multistep movement of the nucleic acid on a molecular substrate interface, the development of autonomous devices has become attractive. The emergence of the DNA walking machine powered by DNA enzymes (Bath et al., 2005; Cha et al., 2014; Wickham et al., 2011) can meet this requirement. With the assistance of such enzymes, the DNA substrate can be autonomously cleaved, without repeated manual operation and cumbersome thermal cycling. In addition, these molecular walking systems can be designed to respond selectively to the special analytes, thereby offering many potential applications in designing different biosensors (Chen et al., 2015b; Jung et al., 2016; Yang et al., 2016b; Zhang et al., 2015).

Mesoporous nanomaterials, such as nanoporous gold (Fan et al., 2015; Fujita et al., 2012; Lang et al., 2013), mesoporous carbon (Kim et al., 2011; Lin et al., 2015; Wang et al., 2016), mesoporous silica (Tang et al., 2012; Tarn et al., 2013; Wang and Gu 2015) and mesoporous platinum (Cui et al., 2016; Cui et al., 2014; Li et al., 2015b), have attracted great research interests recently due to their desirable properties, containing well-defined configuration, excellent electrocatalytic activity, and

remarkable structural thermostability. With these excellent properties, they have become promising candidates for diverse important applications (Cui et al., 2016; Fan et al., 2015; Wang et al., 2016; Yang et al., 2016a; Yu et al., 2016). Among those nanomaterials, Mesoporous Pt nanospheres (MPNs) have received special concerns due to their high pore volume, large surface area, high loading capacity, distinct electrical conductivity, easy functionalization, and superior catalytic activity. Introducing MPNs into electrochemical sensors could efficiently increase the specific biosensing surface and deliver amounts of signal molecules, which could evidently enhance the performances of sensors. On the basis of these distinct properties of MPNs, DNA modified and DOX encapsulated MPNs (MPNs@DOX@DNA) were first synthesized and utilized. In this study, the MPNs were not only employed as nanocarriers for electroactive signal reporter (DOX) and thiol-functionalized DNA, and as electrocatalytic substances for remarkably enhanced sensitivity of the devices.

In this work, we presented a sensitive and universal ratiometric electrochemical biosensing platform for the ultrasensitive detection of various bioanalytes. First, two types of DNA probes were simultaneously immobilized on the Au electrode. In the presence of targets, the terminally protected DNA walkers (DWs) were powered by nicking endonuclease (Nt.BbvCI), and they exhibited autonomous cleavage

behavior on the surface of the substrate DNA-modified electrode. The Nt.BbvCI condition was systematically optimized. To increase the efficiency of signal detection and enhance the dynamics of DWs, we improved the scheme by substituting MB-hairpin probes (MB-HPs) for MB labeled linear DNA probes. Subsequently, the efficiency of Nt.BbvCI and the other critical conditions of the experiment were progressively optimized. In the presence of targets and Nt.BbvCI, MPNs@DOX@DNA2 was tightly anchored on the surface of the electrode through strand displacement reactions (SDRs), Consequently, the MB response was significantly reduced, the DOX signal was increased. The proposed nanocomposite-based signal-off-on ratiometric electrochemical strategy with a detection performance superior to that of the signal-off strategy was established by progressively optimizing the schematics(Fig. S1). This strategy was successfully applied in human serum samples with satisfactory results, which demonstrated its considerable potential in clinical applications.

2. Experimental

2.1. Reagents and materials

All oligonucleotide sequences (Table S1), adenosine triphosphate (ATP), uridine -5'-triphosphate (UTP), cytidine-5'-triphosphate (CTP), guanosine-5'-triphosphate (GTP), and potassium bromide were purchased

from Sangon Biotechnology. Co, Ltd (Shanghai, China). Chloroplatinic acid was obtained from Adamas (Shanghai, China). 6-Mercapto-1-hexanol (MCH) was obtained from Sigma Aldrich (St. Louis, USA). Nt.BbvCI and NE buffer (10×) were ordered from New England Bio-labs, Inc (Beverly, MA, USA). Buffer for electrochemical impedance spectroscopy (EIS): PBS(0.1 M), $[Fe(CN)_6]^{3-/4-}$ (5 mM) and KCl (0.1 M, pH 7.0). Buffer for cyclic voltammetry (CV) and Square Wave Voltammetry (SWV): Tris–HCl (20 mM), NaCl (140 mM, pH 7.4). Ultrapure water (Milli-Q 18.2 MΩ, Millipore System Inc.) was employed in all runs. All other chemicals were of reagent grade and used as received.

2.2. Apparatus and instruments

All electrochemical measurements were performed in an electrochemical workstation (CHI-660E, Shanghai, China). A conventional three-component electrochemical cell, with a modified Au electrode as the working electrode, a KCl-saturated Ag/AgCl electrode as the reference electrode, and a Pt wire as the auxiliary electrode, was employed in all electrochemical measurements. EIS and CV measurements were used to characterize the interface properties of the modified electrode. Transmission electron microscopy (TEM,

Hitachi-7500. Japan) was employed to monitor the structures of the nanomaterials. A Surface area and porosity analyzer (ASAP-2020, USA) was used to characterize the surface area and mesoporous structure of MPNs. X-Ray photoelectronic spectroscopy (XPS, Thermo ESCALAB-250, USA) was employed for elemental analysis to further investigate the successful synthesis of MPNs. Atomic force microscopy (AFM, IPC-208B, Chongqing, China) was performed to observe the images of different modified electrodes. UV visible absorption spectroscopy (Thermo Nanodrop-1000, USA) was used to characterize the synthesized nanocomposites.

3. Results and discussion

3.1. **Principle of the signal-off sensing system based on linear probes**

Scheme 1 illustrates the principle of this signal-off sensing system. Two types of linear nucleic acid probes (thiol-modified MB-DNA1 and DWs) were designed to have a seven-nucleotide (nt) nicking recognition sequence (Yang et al., 2016b) simultaneously immobilized on the Au electrode through Au-S binding. The MB molecules close to the electrode surface were confined for efficient electron transfer. The target-specific aptamers were introduced to partially block the nicking recognition site of DWs. Subsequently, the electrode was incubated with MCH solution to

block the remaining bare area. The aptamers were integrated with the present targets, and they were released from DWs. When the aptamers were released, the nicking recognition sequences of MB-DNA1 and DWs were combined in particular. Therefore, the DWs were powered by Nt.BbvCI and autonomously walked to cleave the specific site on MB-DNA1, which resulted in a large amount of MB molecules distant from the electrode. Additionally, the current response remarkably declined.

< Fig 1>

3.2. Characterization of the electrode

To validate the interface properties of the modified electrode, CV was selected to monitor the stepwise fabrication of this aptasensor. As shown in Fig. 1A, the bare Au electrode showed a couple of strong redox peaks (curve 1), which indicated that the Au electrode possessed excellent electron transfer properties. When the MB-DNA1 and DWs probes were immobilized, the current response sharply decreased (curve 2) due to the negatively charged phosphoric acid backbones produced an electrostatic repulsion force to anionic $[Fe(CN)_6]^{3-/4-}$. Afterward, the lowest redox peaks (curve 3) were obtained after blocking with MCH, because the nonconductive properties of the MCH inhibited the electron transport to the electrode surface. In the presence of targets, the DWs were powered

by Nt.BbvCI and autonomously moved to cleave multiple DNA1 substrates on the electrode. Consequently, the current signal noticeably increased (curve 4). All the CV data demonstrated the success of the stepwise modification.

EIS was also used to monitor the features of this sensing system (Fig. 1B). The bare Au electrode showed a substantially small semicircle domain (curve 1), which demonstrated its excellent electron transfer ability. The impedance increased after immobilization of the mixed probes (curve 2), thereby suggesting that the mixed probes were successfully combined on the electrode surface through Au–S bond. The semicircle further increased when MCH was immobilized on the Au electrode (curve 3). This observation implied that the immobilized MCH inhibited the electron transport to the electrode surface with nonconductive properties. In the presence of targets, the electron transfer resistance remarkably decreased (curve 4) due to the MB-DNA1 substrates were cut and removed from the electrode. The EIS changes agreed with the CV response, which further indicated the success of each modification step.

AFM is an effective and visualized characterization method to verify that two different lengths of probes were simultaneously immobilized on the surface of the electrode (Wang et al., 2015). The three-dimensional height maps of the modified probes were shown in AFM images (Figs.

1C and 1D). A rough and blunt appearance was obtained after modification of only MB-DNA1 (Fig. 1C). The surface mean roughness (Sa) of this electrode was 8.826 nm, and the surface root mean square roughness (Sq) was 10.683 nm. Furthermore, an intensive and towering image was observed when the mixed probes were simultaneously immobilized (Fig. 1D). The Sa of this electrode was 14.796 nm, and the Sq was 19.582 nm. This result is due to the DWs was much longer than MB-DNA1, which proved that two probes with different lengths were successfully immobilized synchronously.

In this study, the current response of the signal-off biosensor was undesirable. We believed that the DWs dynamics was influenced by Nt.BbvCI efficiency, and the efficiency of Nt.BbvCI was affected by the length of nucleic acid at the two sides of nicking recognition site of the MB-DNA1. To verify this hypothesis, we progressively increased the bases of MB-DNA1 from 13 nt to 19 nt. As presented in Fig. 1E, after reaction with targets, the current response noticeably decreased with increasing length, especially at the length of 15 nt. All these results verified that the length of nucleic acid at the two sides of nicking recognition site is a key factor influencing the dynamics of DWs.

3.3. **Principle of the HP-based signal-off sensing system**

With the increasing length of MB-DNA1, the signal molecular MB correspondingly stayed away from the surface of the electrode, which consequently weakened the electron transfer properties. To increase the efficiency of signal detection, and improve the dynamics of DWs simultaneously, we improved the scheme by substituting MB-DNA1 with MB-HP. As shown in scheme 2, the MB was modified at the end of the MB-HPs, and the nicking enzyme recognition sequence was designed at the loop of the MB-HPs. Thus, the MB could be remarkably close to the electrode surface. In addition, the enzyme efficiency could be adjusted by optimizing the size of the loop. The loop was cut as the special recognition and dissection of Nt.BbvCI in the presence of targets. Toehold-induced SDRs were initiated between DNA2 and the cleaved MB-HPs. The MB-oligonucleotide fragments were forced to stay away from the electrode, which resulted in the current response of MB violently released.

< Fig 2>

3.4. Optimization of experimental conditions

To obtain the desired results, critical experimental conditions were prior optimized. First, the loop size of the MB-HPs may be a crucial factor to influencing the dynamics of DWs. As shown in Fig. 2A, in the

presence of targets, the current response remarkably decreased until 21 nt, when the loop size was increased from 17 nt to 25 nt. As the loop size was further increased, the initial current also decreased. In addition, the DW dynamics showed no evident changes and even decreased at 25 nt because the steric hindrance effect released the coverage of probes immobilized on the electrode. Thus, 21 nt was selected as the optimal loop size of the MB-HPs. The sequences and structures of different loop sizes of MB-HPs are shown in Fig. S3.

Given the dual roles of the MB-HPs as both cleavable substrate and the signal-containing unit on the electrode surface, MB-HP concentration is also a possible key factor affecting the response of this biosensor. Considerably low concentrations could influence the response of signal MB. However, substantially high concentrations could also result in the difficult increase of the current response to the steric hindrance effect. Electrochemical signals were measured at different concentrations of the MB-HPs. As shown in Fig. 2B, the current response gradually increased with increasing MB-HP concentration until 1 μM and then slightly decreased with further increase in concentration. This result illustrated that a high surface density of the MB-HPs could cause the steric crowding effect and decrease the DNA hybridization efficiency. Hence, 1 μM was selected as the most optimal concentrations of the MB-HPs used in this study.

The ratio of MB-HPs and DWs is another critical factor to influence the current response. To understand the effect of DWs, we fixed the concentration of the MB-HPs at 1 μM and altered the DWs concentration (200, 100, 67, 50, and 25 nM; DWs : MB-HPs = 1:5, 1:10, 1:15, 1:20, and 1:25). As shown in Fig. 2C, the current response increased with increasing rate, until it reached 1:15, and then decreased. This result is due to that the MB-HPs cannot be cut sufficiently at the low-concentration DWs. High concentrations also generated the steric hindrance effect. Thus, 1:15 was the optimal rate used in this method.

We also studied the effects of Nt.BbvCI concentration in solution to the aptasensor response and the reaction time of Nt.BbvCI. $|\Delta I_{MB}|$ linearly increased with Nt.BbvCI [C] concentration, where [C] ≤ 5 U/100 μL. No obvious $|\Delta I_{MB}|$ alteration was observed with further increase in [C] (Fig. 2E). The effect of Nt.BbvCI interaction time (5-40 min) was also studied (Fig. S4). The current response gradually increased from 5 min to 25min and reached a plateau at 40min. Hence, 5 U was used as the Nt.BbvCI concentration, and 25min was selected as the optimum Nt.BbvCI interaction time.

3.5. **Principle of the signal-off-on ratiometric electrochemical aptasensor**

Electrochemical HP-based biosensors can be realized in either signal-off or signal-on format (Gao et al. 2015; Qian et al. 2015; Wei et al. 2008; Wickham et al. 2011; Wu et al. 2013; Xiong et al. 2015; Zhuang et al. 2013). Correspondingly, the signal either decreases or increases in response to the presence of the analytes. Signal-off electrochemical biosensors are relatively susceptible to false positives, which reduce their limit of detection and dynamic ranges compared with signal-on sensors (Gerasimova and Kolpashchikov 2014). Therefore, we introduced a signal-off-on ratiometric electrochemical strategy to reduce the influence of false positives and improve the efficiency of detection. As illustrated in scheme 3, the MB-HPs acted as a signal-off probe, and MPNs@DOX@DNA2 acted as a conventional signal-on probe. SDR was initiated by the DNA2-functionalized nanocomposites. Consequently, the MB-oligonucleotides were rapidly released, and the nanocomposite-modified sensing interface was obtained. Therefore, the MB response significantly reduced, whereas the DOX signal increased.

<Scheme 3>

3.6. Characterization of the nanomaterials

TEM was employed to characterize the structures of MPNs, as presented in Fig.3A. The nanospheres were well-dispersed and highly

uniform in shape and size. The average size of MPNs was approximately 70 nm, the distribution of unequal-sized pores on the surface was evident, and the mean size was 10 nm. When loaded with DOX (Fig. 3B), the nanoparticle size was almost the same, but the pores were not evident as before. This result indicated that DOX was encapsulated in the pores of MPNs. Moreover, elemental analysis was performed using XPS to further confirm the successful synthesis of MPNs. As shown in Fig. 3C, the characteristic XPS peaks of platinum (51.5, 71, 75.1, 314.5, and 331.2 eV for 5P3/2, 4f7/2, 4f5/2, 4d5/2, and 4d3/2, respectively) were observed. Elemental analysis results verified the successful synthesis of MPNs.

The surface areas and pore size distributions were investigated by N_2 adsorption desorption isotherms. The MPN curves (Fig. 3D) showed a typical type *V* isotherm with a small H3 hysteresis loop, which implied its complex 3D pore connectivity mesostructure. The MPNs showed a wide pore distribution with a BET surface area of 46.141 $m^2\ g^{-1}$ and a pore volume of 0.065 $cm^3\ g^{-1}$. The pore size calculated from the adsorption branch with the BJH method was 11.218 nm (Fig. 3E). The N_2 adsorption–desorption isotherm curves verified the successful synthesis of MPNs with high pore volume, large surface area, and high loading capacity.

To validate whether DNA2 and DOX are both present in the MPNs, we employed UV–vis absorption spectroscopy to characterize the MPN,

DOX, DNA2, and MPNs@DOX@DNA2 nanocomposites (Fig. 3F). Pure DOX showed a characteristic adsorption peak at around 485 nm (red curve), whereas that of DNA2 (blue curve) appeared at 260nm. By contrast, the bare MPNs (black curve) showed no absorption peak. When DOX and DNA2 were assembled with MPNs (purple curve), the UV–vis adsorption peaks of DOX and DNA2 simultaneously appeared. The curve slightly red shifted because of the interparticle plasmon coupling. These results indicated that DOX and DNA2 were tightly bound to MPNs.

<Fig. 3>

3.7. Feasibility of the ratiometric electrochemical biosensor

The SWV responses of the different modified electrodes were measured to demonstrate the feasibility of the proposed signal-off-on aptasensor. As shown in Fig. S5, when the MB-HPs were immobilized, only a well-defined current peak of MB at approximately -0.312 V was measured because the MB molecule efficiently transferred the electrode (curve a). The MB response was significantly reduced, whereas the DOX response increased (curve b) when the modified Au electrode was further incubated with Nt.BbvCI in the presence of ATP. This result was largely due to that the MB-HPs were damaged. As the special recognition and

dissection of Nt.BbvCI, the MB modified oligonucleotides were substituted with MPNs@DOX@DNA2. By contrast, the redox currents of MB and DOX slightly changed in the absence of ATP because MPNs@DOX@DNA2 was unable to react with the MB-HPs without the ATP (curve c). The current response showed no evident change in the absence of Nt.BbvCI (curve d), because the Nt.BbvCI failed to power the DWs. Consequently, MPNs@DOX@DNA2 was unable to anchor on the electrode. Furthermore, the feasibilities of the proposed signal-off-on VEGF aptasensor and rpoB gene biosensor were investigated (Figs. S6 and S7). The above results suggested that this ratiometric electrochemical aptasensor produced a readily measured current variation that could be related to the presence and concentration of targets.

3.8. Analytical performance and selectivity of the aptasensor

ATP, VEGF, and rpoB gene at different concentrations were analyzed under the optimized experimental conditions to investigate the general applicability of the proposed universal ratiometric sensing system. We first evaluated the capacity of the proposed method to detect ATP. As shown in Fig. 4A, the MB current decreased, and the DOX current increased monotonically as the ATP concentration was increased from 10 pM to 1 μM. $|\Delta I_{DOX}|+|\Delta I_{MB}|$ was used as the response signal to determine

the concentration of ATP quantitatively. The value of $|\Delta I_{DOX}|+|\Delta I_{MB}|$ was linear with the logarithm of ATP concentration. The regression equation was expressed as y=3.669C+21.74, with a coefficient of determination (R^2) of 0.998, where C is ATP concentration (n=3). The detection limit was 3 pM (S/N=3). Compared with the variation in individual MB current, the logarithm of ATP concentration was analyzed on the basis of the individual MB signals (Fig. S8A). Although the resulting calibration curves also exhibited a linear relationship (Fig. S8B), the double-signal results indicated excellent performance in terms of analytical range and detection limit.

The ratiometric aptasensor also demonstrated a high specificity to ATP when the ATP analogues, GTP, CTP, and UTP were used. Different current response signals were obtained from solutions containing ATP (1.0 μM and 0 M), GTP (1.0 μM), CTP (1.0 μM), and UTP (1.0 μM) under the same experimental conditions. The current value showed no apparent changes, except in the ATP-containing solutions. Therefore, GTP,CTP, and UTP could not interfere with ATP detection. This result evidently indicated that the proposed strategy possessed sufficient specificity for ATP detection, and it could detect ATP among its analogs.

To change the aptamer sequence, VEGF was selected as an example of the ratiometric protein aptasensor. We detected the VEGF with

concentrations ranging from 0.1 pg mL^{-1} to 1000 pg mL^{-1} (Fig. 4B). The electrochemical current increased with increasing VEGF concentration. The $|\Delta I_{DOX}|+|\Delta I_{MB}|$ value was linear with the VEGF concentration. The regression equation was expressed as y=0.022C+2.986, with an R^2 of 0.999, where C is the VEGF concentration (n=3). The detection limit was 0.1 pg mL^{-1} (S/N=3). Moreover, as shown in the remarkable difference in signal for VEGF and noncognate target leptomycin B and Epicerura pergrisea virus (EPV), the proposed aptasensor showed remarkably high selectivity with no obvious interference from the two other proteins.

We also detected the rpoB gene of Mycobacterium tuberculosis (Miodek et al., 2015) as an example of the ratiometric DNA sensor. We analyzed the rpoB gene with concentrations ranging from 1 fM to 100 nM (Fig. 4C). The electrochemical current showed no remarkable increase with increasing concentration of the rpoB gene. The $|\Delta I_{DOX}|+|\Delta I_{MB}|$ value was linear with the concentration of the rpoB gene. The regression equation was expressed as y=2.499C+18.046, with an R^2 of 0.998, where C is the concentration of the rpoB gene (n=3). The detection limit was 0.6 fM (S/N=3). When we detected one-base mutation (T-1), two-base mutation (T-2), and complete-mutation DNA (Cm), the signal was considerably lower than that of the target rpoB gene. This observation revealed that single-base mutation could be obviously distinguished,

indicating that the ratiometric DNA sensor also exhibited excellent specificity.

<Fig.4>

3.9. Stability and reproducibility of the aptasensor

The ratiometric electrochemical biosensor was incubated with ATP (0.5 nM), VEGF (700 pg ml^{-1}), and rpoB gene (100 nM). The aptasensor stability was evaluated every 3 days for storage at 4 °C. The biosensor retained 86.46%, 89.77% and 92.84% of its initial current response, after a storage period of 12 days with ATP, VEGF, and rpoB gene, respectively (Fig. S9). This result indicated that the aptasensor exhibited a good and long-term stability. The reproducibility was investigated by using four electrodes incubated with the same concentration of analytes. As shown in Fig. S10, the RSD values were 5.684%, 3.043%, and 4.96%. Therefore, the proposed aptasensor also possessed acceptable reproducibility.

3.10. Application in serum samples

To evaluate the analytical reliability of the proposed aptasensor, we detected the analytes in normal human serum samples (provided by the No.2 Peoples' Hospital of Yibin, Sichuan). Assays were performed by spiking the serum samples diluted 10 times with different concentrations of ATP, VEGF, and rpoB gene. The detection procedures were the same as that for clean PBS or TE buffer solution. The recovery rate was also calculated on the basis of the calibration curves performed in the buffer. The recovery results agreed with the spiked amounts of targets (Table 1). The slight difference between the measured and actual values could be due to the effect of the serum samples because the collected serum contained a small amount of analytes. The results proved that the precision and recovery of the proposed method applied in complex biological samples were satisfactory. Furthermore, the clinical application and transformation should be investigated in future works.

< Table 1>

4. Conclusion

We established a sensitive and universal ratiometric electrochemical biosensing platform by progressively optimizing the schematics. This ratiometric electrochemical device provided several unprecedented advantages. First, the MPNs were employed as nanocarriers for electroactive signal reporter (DOX) and thiol-functionalized DNA and as

electrocatalytic activity substances for remarkably enhanced sensitivity of devices. Second, two types of DNA probes were simultaneously immobilized on the Au electrode. The terminally protected DWs were powered by Nt.BbvCI, and they exhibited autonomous cleavage behavior, which required no repeated manual operations and cumbersome thermal cycling. Numerous nonspecific signals were reduced, which rendered the proposed method cost efficient and practical for clinical applications. Furthermore, the proposed universal ratiometric electrochemical assay could analyze different targets by changing the molecular recognition elements depending on the target. Under the optimum experimental conditions, the proposed universal ratiometric electrochemical biosensor showed a high sensitivity with a broad detection range to different biomolecules, including small molecules, nucleic acids, and proteins. This biosensor also realized well-accepted signal response in identifying serum samples, thereby resulting in a wide prospect for bioanalysis and clinical diagnosis.

Acknowledgments

This work was financially supported by the Natural Science Research Foundation of China (81171415, 81672112) and the Chongqing Yuzhong District Science and Technology Project (20140108)

References

Banerjee, R., Teng, C.B., Cunningham, S.A., Ihde, S.M., Steckelberg, J.M., Moriarty, J.P., Shah, N.D., Mandrekar, J.N., Patel, R., 2015. Clin. Infect. Dis. 61(7), 1071-1080.

Bath, J., Green, S.J., Turberfield, A.J., 2005. Angew. Chem. 44(28), 4358-4361.

Berg, B., Cortazar, B., Tseng, D., Ozkan, H., Feng, S., Wei, Q., Chan, R.Y.-L., Burbano, J., Farooqui, Q., Lewinski, M., 2015. ACS nano 9(8), 7857-7866.

Carta, S., Penco, F., Lavieri, R., Martini, A., Dinarello, C.A., Gattorno, M., Rubartelli, A., 2015. P. Natl. Acad. Sci. 112(9), 2835-2840.

Cha, T.G., Pan, J., Chen, H., Salgado, J., Li, X., Mao, C., Choi, J.H., 2014. Nat. Nanotechnol. 9(1), 39-43.

Chen, C., Liu, Y., Zheng, Z., Zhou, G., Ji, X., Wang, H., He, Z., 2015a. Anal. Chim. Acta. 880, 1-7.

Chen, Y., Xiang, Y., Yuan, R., Chai, Y., 2015b. Nanoscale. 7(3), 981-986.

Cui, H.-F., Bai, Y.-F., Wu, W.-W., He, X., Luong, J.H., 2016. J. Electroanal. Chem. 766, 52-59.

Cui, Z., Wu, D., Zhang, Y., Ma, H., Li, H., Du, B., Wei, Q., Ju, H., 2014. Anal. Chim. Acta. 807, 44-50.

Dadrich, M., Nicolay, N.H., Flechsig, P., Bickelhaupt, S., Hoeltgen, L., Roeder, F., Hauser, K., Tietz, A., Jenne, J., Lopez, R., 2016. OncoImmunology, e1123366.

Das, J., Ivanov, I., Montermini, L., Rak, J., Sargent, E.H., Kelley, S.O., 2015. Nat. Chem. 7(7), 569-575.

Dopico, X.C., Evangelou, M., Ferreira, R.C., Guo, H., Pekalski, M.L., Smyth, D.J., Cooper, N., Burren, O.S., Fulford, A.J., Hennig, B.J., 2015. Nat. Commun. 6.

Fan, H., Guo, Z., Gao, L., Zhang, Y., Fan, D., Ji, G., Du, B., Wei, Q., 2015. Biosens. Bioelectro. 64, 51-56.

Fujita, T., Guan, P., McKenna, K., Lang, X., Hirata, A., Zhang, L., Tokunaga, T., Arai, S., Yamamoto, Y., Tanaka, N., 2012. Nat. mater. 11(9), 775-780.

Gao, F., Qian, Y., Zhang, L., Dai, S., Lan, Y., Zhang, Y., Du, L., Tang, D., 2015. Biosens. Bioelectro. 71, 158-163.

Gerasimova, Y.V., Kolpashchikov, D.M., 2014. Che. Soc Rev. 43(17), 6405-6438.

Innis, M.A., Gelfand, D.H., Sninsky, J.J., White, T.J., 2012. Academic press.

Jung, C., Allen, P.B., Ellington, A.D., 2016. Nat. Nanotechnol. 11(2), 157-163.

Kelley, S.O., Mirkin, C.A., Walt, D.R., Ismagilov, R.F., Toner, M., Sargent, E.H., 2014. Nat. nanotechnol. 9(12), 969-980.

Kim, M.I., Ye, Y., Won, B.Y., Shin, S., Lee, J., Park, H.G., 2011. Adv. Funct. Mater. 21(15), 2868-2875.

Lang, X.-Y., Fu, H.-Y., Hou, C., Han, G.-F., Yang, P., Liu, Y.-B., Jiang, Q., 2013. Nat commun. 4.

Li, T., Liu, L., Li, Y., Xie, J., Wu, H.C., 2015a. Angewandte Chemie. 54(26), 7568-7571.

Li, Y., Bastakoti, B.P., Malgras, V., Li, C., Tang, J., Kim, J.H., Yamauchi, Y., 2015b. Angew. Chem. Internat. Edit. 54(38), 11073-11077.

Lin, M., Song, P., Zhou, G., Zuo, X., Aldalbahi, A., Lou, X., Shi, J., Fan, C., 2016. Nat. Protoc. 11(7), 1244-1263.

Lin, T., Chen, I.-W., Liu, F., Yang, C., Bi, H., Xu, F., Huang, F., 2015. Science. 350(6267), 1508-1513.

Linardy, E.M., Erskine, S.M., Lima, N.E., Lonergan, T., Mokany, E., Todd, A.V., 2016. Biosens. Bioelectro. 75, 59-66.

Liu, R., Wang, X., Aihara, K., Chen, L., 2014. Med. Res. Rev. 34(3), 455-478.

Loh, P.-R., Bhatia, G., Gusev, A., Finucane, H.K., Bulik-Sullivan, B.K., Pollack, S.J., de Candia, T.R., Lee, S.H., Wray, N.R., Kendler, K.S., 2015. Nat. Genet.

Miodek, A., Mejri, N., Gomgnimbou, M., Sola, C., Korri-Youssoufi, H., 2015. Anal. Chem. 87(18), 9257-9264.

Onda, T., Inoue, K., Suwa, S., Nishizaki, Y., Kasai, T., Kimura, Y., Fukuda, K., Okai, I., Fujiwara, Y., Matsuoka, J., 2016. Int. J. Cardiol. 219, 180-185.

Petersen, O.H., Verkhratsky, A., 2016. R. Soc. B. 371(1700), 20150418.

Pletscher-Frankild, S., Pallejà, A., Tsafou, K., Binder, J.X., Jensen, L.J., 2015. Methods. 74, 83-89.

Qian, Y., Tang, D., Du, L., Zhang, Y., Zhang, L., Gao, F., 2015. Biosens. Bioelectro. 64, 177-181.

Sawyers, C.L., 2008. Nature. 452(7187), 548-552.

Shibuya, M., 2013. J. Biochem. 153(1), 13-19.

Sreekumar, A., Poisson, L.M., Rajendiran, T.M., Khan, A.P., Cao, Q., Yu, J., Laxman, B., Mehra, R., Lonigro, R.J., Li, Y., 2013. Nature. 499(7459), 504-504.

Tang, F., Li, L., Chen, D., 2012. Adv. Mater. 24(12), 1504-1534.

Tarn, D., Ashley, C.E., Xue, M., Carnes, E.C., Zink, J.I., Brinker, C.J., 2013. Accounts Chem. Res. 46(3), 792-801.

Toh, S.Y., Citartan, M., Gopinath, S.C., Tang, T.-H., 2015. Biosens. Bioelectro. 64, 392-403.

Tsai, C.-L., Koong, A.C., Hsu, F.-M., Graber, M., Chen, I.-S., Cheng, J.-H., 2013. Oncology. 84(Suppl. 1), 64-68.

Wang, G.H., Cao, Z., Gu, D., Pfänder, N., Swertz, A.C., Spliethoff, B., Bongard, H.J., Weidenthaler, C., Schmidt, W., Rinaldi, R., 2016. Angew. Chem. Internat. Edit. 55(31), 8850-8855.

Wang, T., Zhang, Z., Li, Y., Xie, G., 2015. Sensor.Actuat. B-Chem. 221, 148-154.

Wang, Y., Gu, H., 2015. Adv. Mater. 27(3), 576-585.

Wei, F., Wang, J., Liao, W., Zimmermann, B.G., Wong, D.T., Ho, C.-M., 2008. Nucleic Acids Res. 36(11), e65-e65.

Wickham, S.F., Endo, M., Katsuda, Y., Hidaka, K., Bath, J., Sugiyama, H., Turberfield, A.J., 2011. Nat. Nanotechnol 6(3), 166-169.

Wu, L., Zhang, X., Liu, W., Xiong, E., Chen, J., 2013. Anal. chem. 85(17), 8397-8402.

Wu, Y.X., Zhang, X.B., Zhang, D.L., Zhang, C.C., Li, J.B., Wu, Y., Song, Z.L., Yu, R.Q., Tan, W., 2016. Anal. Chem. 88(3), 1639-1646.

Xiong, E., Zhang, X., Liu, Y., Zhou, J., Yu, P., Li, X., Chen, J., 2015. Anal. Chem 87(14), 7291-7296.

Yang, X., Tang, Y., Mason, S.D., Chen, J., Li, F., 2016b. ACS Nano .10(2), 2324-2330.

Yu, C., Qian, L., Ge, J., Fu, J., Yuan, P., Yao, S.C., Yao, S.Q., 2016. Angewandte Chemie. 55(32), 9272-9276.

Zhang, H., Lai, M., Zuehlke, A., Peng, H., Li, X.-F., Le, X.C., 2015. Angew. Chem. Internat. Edit. 54(48), 14326-14330.

Zheng, D., Zou, R., Lou, X., 2012. Anal. Chem. 84(8), 3554-3560.

Zhu, Y., Hu, X.C., Shi, S., Gao, R.R., Huang, H.L., Zhu, Y.Y., Lv, X.Y., Yao, T.M., 2016. Biosens. Bioelectr. 79, 205-212.

Zhuang, J., Fu, L., Tang, D., Xu, M., Chen, G., Yang, H., 2013. Biosens. Bioelectro. 39(1), 315-319.

Scheme 1. Principle of the signal-off sensing system based on linear probes. (A) CV for different modified electrodes. (B) Nyquist plot for ESI measurements for different modified electrodes: bare Au electrode (1); MB-DNA1, DWs/Au electrode (2); MB-DNA1, DWs/MCH/Au electrode (3); target, Nt.BbvCI/MB-DNA1, DWs/MCH/Au electrode (4). (C) AFM images for the MB-DNA1 immobilized Au electrode; (D) AFM images for the MB-DNA1 and DWs were simultaneously immobilized Au electrode. (E) SWV signal curves responding to different length of MB-DNA1, and the sequence of different length of MB-DNA1 : "**" represents the cutting site of Nt.BbvCI, red region represents the nicking recognized sequence.

Scheme 2. Principle of the signal-off sensing system based on hairpin probes. (A) The SWV for optimizing the loop size of MB-HPs from 17 nt to 25 nt; (B) MB-HPs concentrations; (C) the ratio of DWs and MB-HPs; (D) the concentration of Nt.BbvCI on the electrochemical response in this sensing system. When one parameter changed, the others kept on their optimal conditions. The target ATP concentration was 1 μM. Error bars represented standard deviations of the measurements (n=3).

Scheme 3. Schematic of the ratiometric electrochemical aptasensor. (A) Preparation procedure of MPNs@DOX@DNA2; (B) Fabrication process of the signal-off-on ratiometric electrochemical aptasensor.

Fig 1. Principle of the signal-off sensing system based on linear probes. (A) CV for different modified electrodes. (B) Nyquist plot for ESI measurements for different modified electrodes: bare Au electrode (1); MB-DNA1, DWs/Au electrode (2); MB-DNA1, DWs/MCH/Au electrode (3); target, Nt.BbvCI/MB-DNA1, DWs/MCH/Au electrode (4). (C) AFM images for the MB-DNA1 immobilized Au electrode; (D) AFM images for the MB-DNA1 and DWs were simultaneously immobilized Au electrode. (E) SWV signal curves responding to different length of MB-DNA1, and the sequence of different length of MB-DNA1 : "**"

represents the cutting site of Nt.BbvCI, red region represents the nicking recognized sequence.

Fig 2. Principle of the signal-off sensing system based on hairpin probes. (A) The SWV for optimizing the loop size of MB-HPs from 17 nt to 25 nt; (B) MB-HPs concentrations; (C) the ratio of DWs and MB-HPs; (D) the concentration of Nt.BbvCI on the electrochemical response in this sensing system. When one parameter changed, the others kept on their optimal conditions. The target ATP concentration was 1 μM. Error bars represented standard deviations of the measurements (n=3).

Fig. 3 (A) TEM images of MPNs; (B) TEM images of MPNs@DOX; (C) The XPS spectra of MPNs; (D) N2 adsorption-desorption isotherms of MPNs; (E) Pore-size distributions of MPNs; (F) UV–vis absorption spectra of MPNs@DOX@DNA2 synthesized.

Fig. 4 Analytical performance of the ratiometric electrochemical biosensor. (A) SWVs of the signal-off-on system with the increasing concentrations of ATP (from 10 pM to 1 μM), calibration curve of $|\Delta I_{DOX}|+|\Delta I_{MB}|$ versus the logarithm of ATP concentrations, and the specificity of ATP aptasensor. (B) VEGF aptasensor system with the increasing concentrations of VEGF (from 0.1 to 1000 pg ml^{-1}), calibration curve of $|\Delta I_{DOX}|+|\Delta I_{MB}|$ versus the

concentrations of VEGF, and the specificity of VEGF aptasensor. (C) rpoB gene biosensor system with the increasing concentrations of rpoB gene (from 1 fM to 100 nM), calibration curve of $|\Delta I_{DOX}|+|\Delta I_{MB}|$ versus the concentrations of rpoB gene, and the specificity of rpoB gene aptasensor. T-1: one base mutation; T-2: two bases mutation; Cm: completely mismatched. Error bars represented standard deviations of the measurements (n=3).

Table 1 Determination results of ATP, VEGF and rpoB gene in serum samples (n=3).

Samples	**Add**	**measured**	**Recovery (%)**	**RSD (%)**
ATP	800 nM	793.333 nM	99.167	2.366
ATP	1 nM	1.057 nM	105.667	5.545
ATP	10 pM	9.206 pM	92.065	6.85
VEGF	1000 pg ml^{-1}	1012.667 pg ml^{-1}	100.127	0.559
VEGF	350 pg ml^{-1}	353.208 pg ml^{-1}	100.982	1.645
VEGF	1 pg ml^{-1}	1.123 pg ml^{-1}	112.3	5.952
rpoB gene	100 nM	94.548 nM	94.548	2.22
rpoB gene	100 pM	92.395 pM	92.395	4.031
rpoB gene	50 fM	52.751 fM	105.501	2.911

Scheme 1

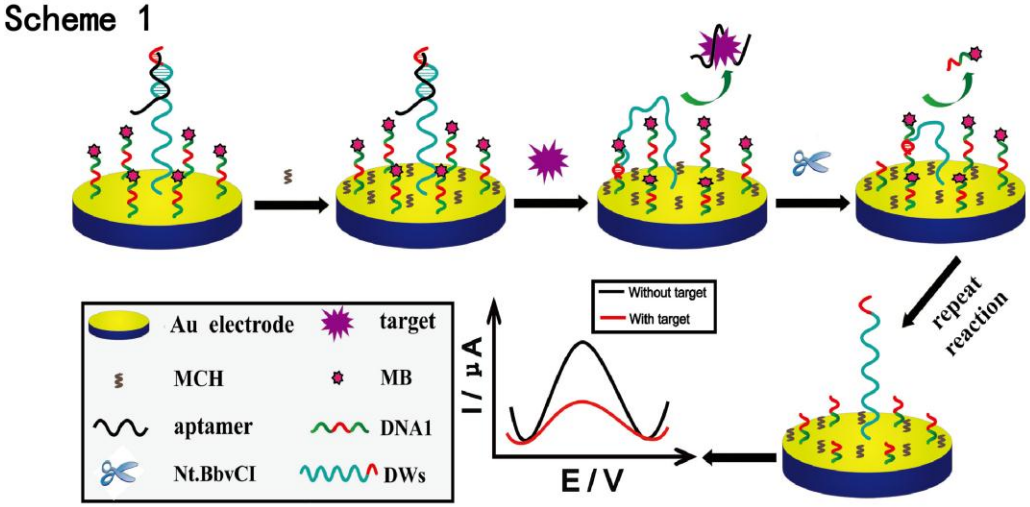

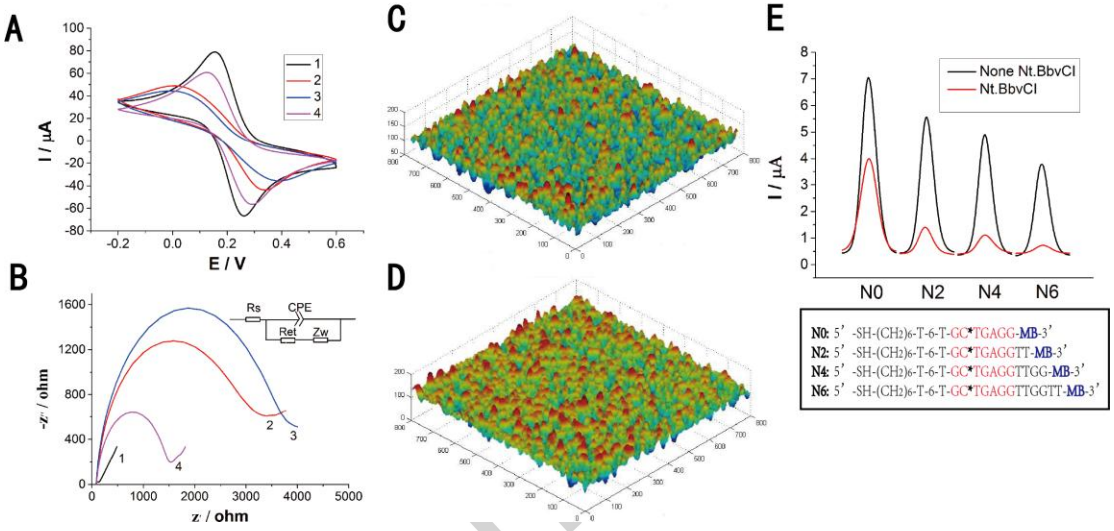

N0: 5' -SH-(CH2)6-T-6-T-GC*TGAGG-MB-3'
N2: 5' -SH-(CH2)6-T-6-T-GC*TGAGGTT-MB-3'
N4: 5' -SH-(CH2)6-T-6-T-GC*TGAGGTTGG-MB-3'
N6: 5' -SH-(CH2)6-T-6-T-GC*TGAGGTTGGTT-MB-3'

Scheme 2

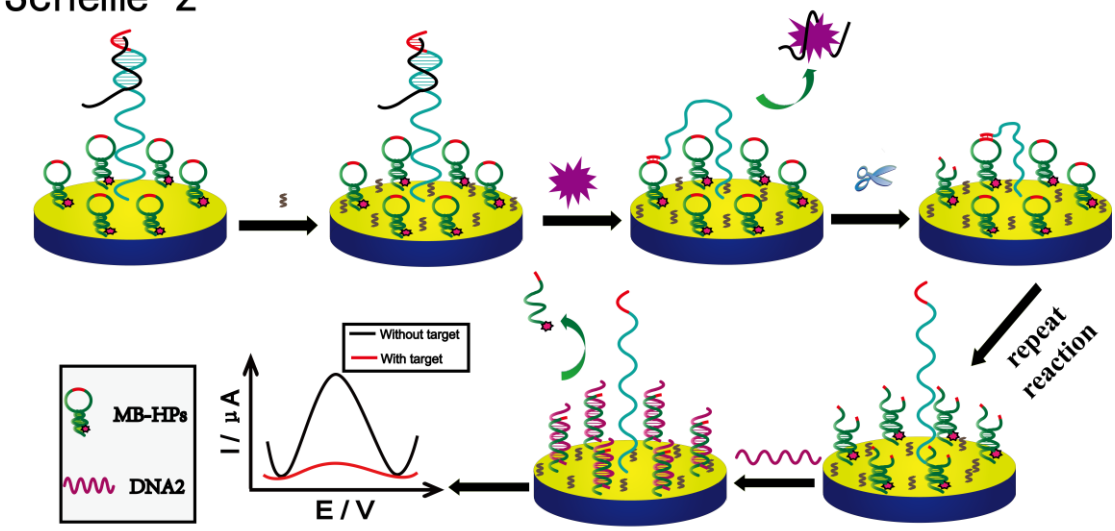

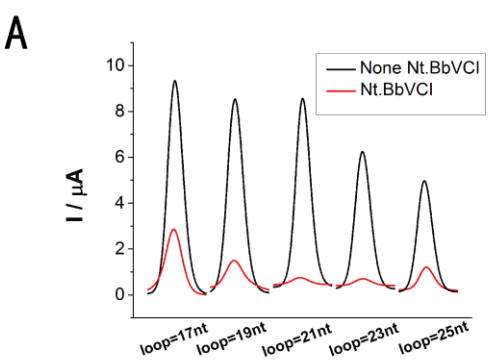

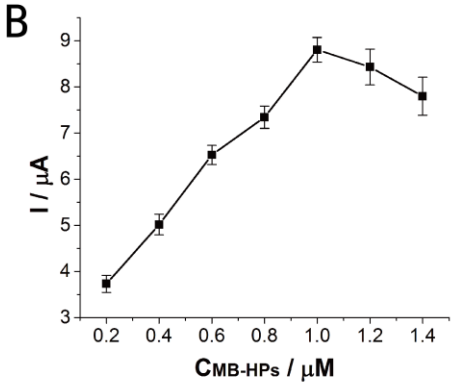

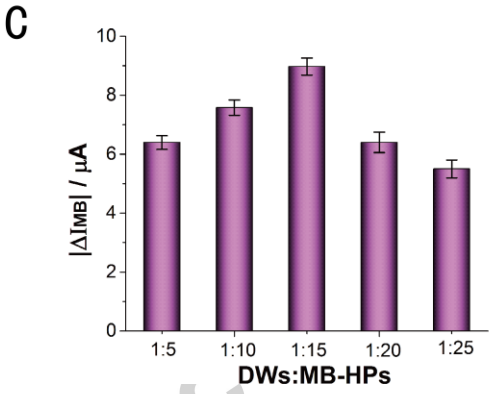

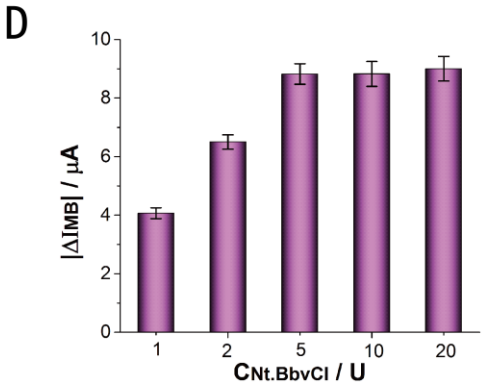

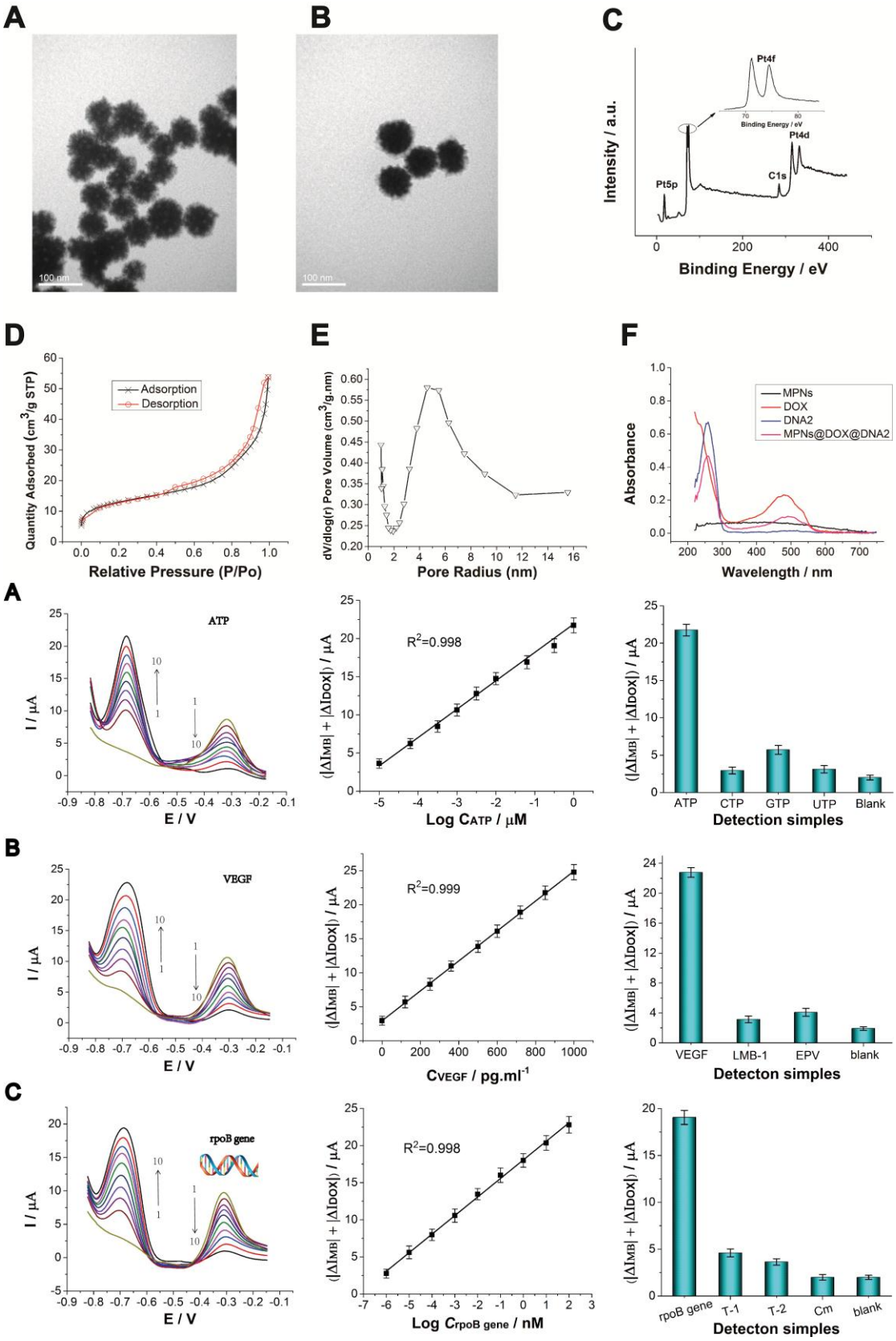

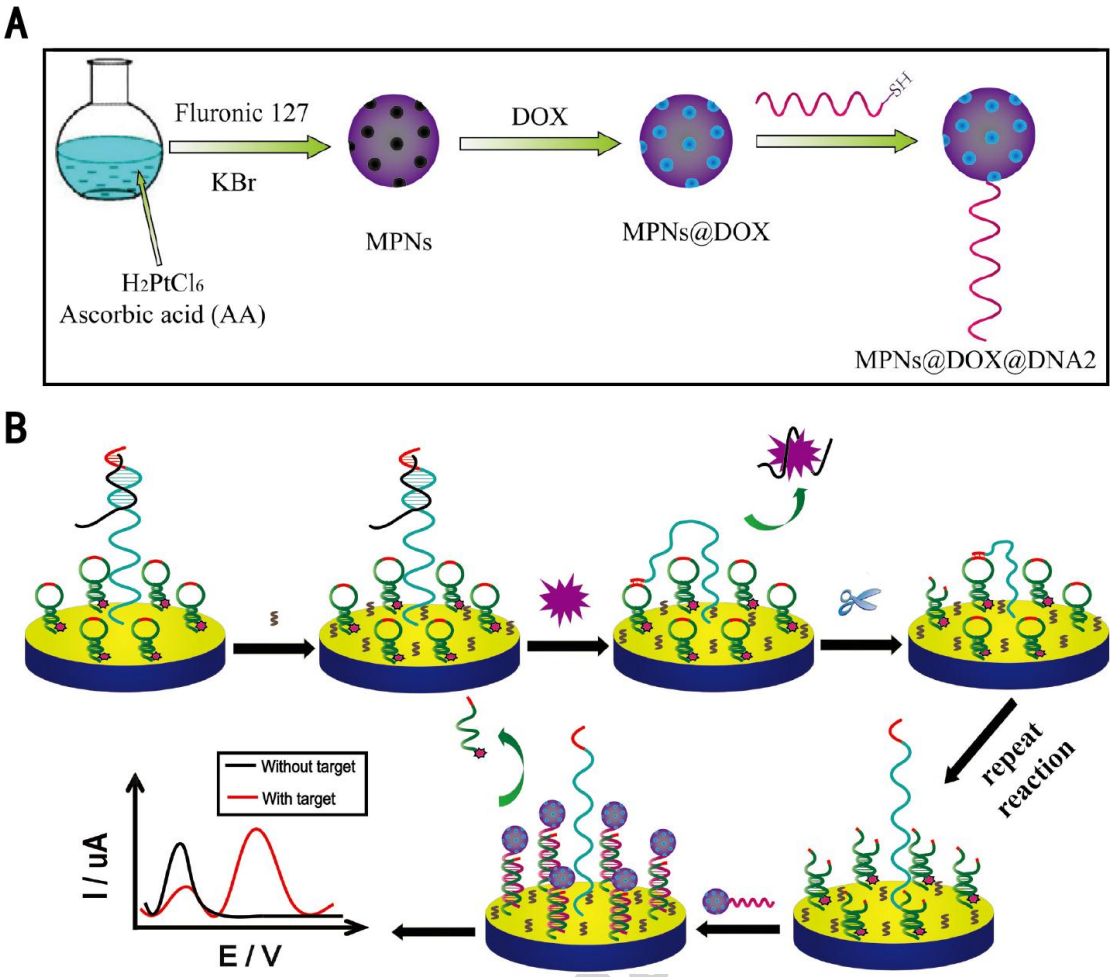

Highlights

- A sensitive and universal ratiometric electrochemical biosensing platform was established by progressively optimizing the schematics.
- Mesoporous platinum was firstly employed in electrochemical aptasensor as nanocarriers and electrocatalytic activity substance for remarkably enhanced the sensitivity.

- Two kinds of DNA probes were simultaneously immobilized on the Au electrode, the terminally protected DWs were powered by Nt.BbvCI and exhibited autonomous cleavage behavior for signal amplification.

- The proposed universal ratiometric electrochemical assay can be utilized to detect diverse targets quantitatively by simply changing the molecular recognition elements according to its targets.